
BENCHMARKING SCIENTIFIC MACHINE LEARNING MODELS FOR AIR QUALITY DATA *

Khawja Imran Masud^{id}
University of North Texas
76205 Texas, USA
KhawjaImran.Masud@unt.edu

Venkata Sai Rahul Unnam
University of North Texas
76205 Texas, USA
VenkataSaiRahulUnnam@my.unt.edu

Sahara Ali^{id}
University of North Texas
76205 Texas, USA
sahara.ali@unt.edu

ABSTRACT

Accurate air quality index (AQI) forecasting is essential for the protecting public health in rapidly growing urban regions, and the practical model evaluation and selection are often challenged by the lack of rigorous, region-specific benchmarking on standardized datasets. Physics-guided machine learning and deep learning models could be a good and effective solution to resolve such issues with more accurate and efficient AQI forecasting. This research study presents an explainable and comprehensive benchmark that enables a guideline and proposed physics-guided best model by benchmarking classical time-series, machine-learning, and deep-learning approaches for multi-horizon AQI forecasting in North Texas (Dallas County). Using publicly available U.S. Environmental Protection Agency (EPA) daily observations of air quality data from 2022 to 2024, we curate city-level time series for $PM_{2.5}$ and O_3 by aggregating station measurements and constructing lag-wise forecasting datasets for $LAG \in \{1, 7, 14, 30\}$ days. For benchmarking the best model, linear regression (LR), SARIMAX, multilayer perceptrons (MLP), and LSTM networks are evaluated with the proposed physics-guided variants (MLP+Physics and LSTM+Physics) that incorporate the EPA breakpoint-based AQI formulation as a consistency constraint through a weighted loss. Experiments using chronological train-test splits and error metrics MAE, RMSE showed that deep-learning models outperform simpler baselines, while physics guidance improves stability and yields physically consistent pollutant with AQI relationships, with the largest benefits observed for short-horizon prediction and for $PM_{2.5}$ and O_3 . Overall, the results provide a practical reference for selecting AQI forecasting models in North Texas and clarify when lightweight physics constraints meaningfully improve predictive performance across pollutants and forecast horizons.

Keywords Scientific Machine Learning, Physics-informed Neural Networks, Air Quality Index, Air Pollution.

1 Introduction

Air quality monitoring and management is a key public health issue, especially in fast-growing urban and industrial centers. The North Texas region, with decades of high population growth and economic development, is faced with chronic air quality problems associated with industrial emissions, increased vehicular traffic, and ozone formation. Poor air quality is a direct human health factor leading to an increase in respiratory ailments, cardiovascular diseases, and other severe health conditions, especially in the vulnerable population [1, 2]. This important regional challenge requires the development of sophisticated analytical tools that accurately model, predict, and help to mitigate events of air pollution [3, 4]. Traditional methods of environmental modeling are often not able to capture the complex nature of the atmospheric data that is non-linear and high-dimensional [4]. In response, increasingly more of the scientific community uses machine learning (ML) to analyze and predict environmental phenomena. ML algorithms are good at analyzing large and heterogeneous data, detecting subtle patterns, and can predict the air quality better than many conventional models [3, 5]. More recently also, the field of Scientific Machine Learning (SciML) has appeared, which integrates domain-specific knowledge (such as the physical principles of atmospheric chemistry) directly in

* Corresponding Author Email: sahara.ali@unt.edu

the model architecture [6, 7]. This hybrid approach like Physics-Informed Neural Networks (PINNs) and stochastic advection-diffusion models, has a high potential to achieve more robust, interpretable, and physically plausible results in the case of complex problems in environmental science, such as the analysis of air pollution. [8, 2].

Despite the increasing use of ML and SciML models, a critical gap has persisted, i.e., the absence of rigorous and region-specific benchmarking. Researchers and policymakers often struggle with choosing the best model for a particular goal, e.g., ozone (O_3) prediction, particulate matter ($PM_{2.5}$) prediction, or data imputation, due to the lack of direct comparative studies performed on a standardized set of data [1, 4]. This research fills this gap by performing an extensive benchmark of the state-of-the-art SciML approaches using a specialized dataset for air quality in North Texas. The major contributions of this research are threefold:

1. The curation of a comprehensive, multi-source environmental dataset for the Dallas region;
2. Proposed and implemented physics-informed SciML models MLP+Physics and LSTM+Physics for air quality time-series forecasting; and
3. A comparative evaluation of these methods using multiple performance metrics.

The Related Study section presents an organized summary of existing literature in the area pertinent to the current research in an attempt to place the proposed research in the context of the broader air quality modeling and forecasting literature. It first reviews the current methodologies for air quality monitoring and prediction, which include the traditional statistical models, machine learning techniques, and recent SciML frameworks. The section then draws attention to commonly used datasets and sources of data, motivating the choice of design described in the Dataset Description section. Next, it discusses methodological trends and limitations in existing studies that help inform model selection and experimental design, which are presented in the Methodology section. Finally, the literature identifies gaps in comparative evaluation and benchmarking at the regional level, which provide the foundation for the Results and Comparative Analysis section and incentive for the broader discussion and conclusions about the results in the final sections of this paper.

2 Related Study

Air pollution, in particular, fine particulates ($PM_{2.5}$) and ozone (O_3) at high concentrations, is a major threat to human health and the environment [9, 10, 11]. Accurately predicting the Air Quality Index (AQI) or concentrations of important pollutants is important to public health warnings, urban planning, and environmental policy. Over decades, different approaches have been used to forecast AQI and pollutants, from basic statistical models to advanced ML, DL, and, more recently, physics-informed scientific ML.

In the early stages of this research, statistical regressions and time-series models were the methods used to predict pollution levels or AQI [12, 13, 14, 15]. These models generally used to use past concentrations of pollutants and meteorological variables to predict future air quality. While good at capturing short-term linear relations, they had difficulties with non-linear dynamics, sudden spikes, and complex pollutant-meteorology interactions characteristic of urban environments. However, their predictive capability was poor, which was the motivation behind moving toward more flexible data-driven approaches.

With the development of multi-pollutant monitoring networks and better data availability, machine learning (ML) [16] presented a new and interesting alternative to classical statistical methods. ML techniques, such as Random Forest, Gradient Boosting Machines, Support Vector Regression, and CatBoost, showed enormous performance in modeling non-linear relationships between pollutants, meteorology, and emission activities. Li et al. [17] have used a Random Forest model to estimate $PM_{2.5}$ concentration on a daily basis in the Huaihai Economic Zone based on satellite AOD, weather data, and spatial-temporal features. The model performed well ($R^2 = 0.85$, RMSE = 14.63 $\mu\text{g}/\text{m}^3$) and generated 1-km maps of pollution and trends over time. However, due to the limitation of Random Forest to capture complex nonlinear or long-range temporal patterns, the performance of the Random Forest model in modeling the fast-changing atmospheric conditions is limited, which demonstrates the necessity of more advanced methods of deep learning. Another research study by Ravindiran et al. [18] used several machine-learning models predict AQI in Visakhapatnam. CatBoost has the best results and very high accuracy ($R^2 \approx 0.9998$, RMSE ≈ 0.76), and significantly better results than traditional methods. This indicates that ML models have the ability to capture the complex relationships in AQI data.

However, these models remain statistical models and do not involve the actual physics of the atmosphere. Because of this, they can sometimes work very well on past data but can be less reliable on unusual weather/climate changes and/or limited data. Similarly, Natarajan et al. [4] proposed an optimized ML approach using Grey Wolf Optimization combined with a Decision Tree regressor and achieved high accuracies (88.98%–97.68%) in their proposed framework

for major cities in India compared to SVR and Random Forest by the use of better feature selection and dealing with class imbalance. In addition to this, a hybrid Random Forest-ARIMA model was proposed for AQI forecasting by Yenikar et al. [5] in which Random Forest was used to capture the non-linear pollutant interactions, and an ARIMA model was used to account for the remaining temporal patterns. This hybrid approach improved anticipatory stability and interpretability compared to standalone ML models, although it remained bounded by its reliance on historical correlations. Nevertheless, despite these advancements, this model also relies predominantly on historical data correlations and struggles to capture intricate temporal dependencies, suggesting that more advanced deep-learning models need to enhance robustness and generalization in AQI prediction.

However, more expressive temporal and spatio-temporal models have great potential in improving air-quality forecasting beyond classical ML, as observed in recent deep learning literature. Early hybrid works like Sarkar et al. [19] who used LSTM and GRU together for AQI prediction in Delhi and found that they achieved low MAE and a higher R2 compared to DL and ML baselines, have already suggested recurrent architectures to be better fit for the capturing of the pollutant dynamics, which are non-linear over time. Building on this, Elbaz et al. [20] proposed a 3D-CNN-GRU model coupled with an attention mechanism in Chemosphere to realize multi-horizon prediction from the image-based and environmental inputs. It has been demonstrated that the joint modeling of spatial texture and temporal evolution can help to obtain a more accurate $PM_{2.5}$ prediction than the conventional CNN or RNN models. More recently, a number of studies of varying quality from 2024-2025 have discussed ever more sophisticated architectures that use hybrids and attention. For example, Nguyen et al. [21] proposed an attention-CNN integrated with a QPSO-based LSTM framework, which greatly improved the performance in predicting daily AQI in Seoul in terms of RMSE and MAE, which is the first to demonstrate the importance of attention and metaheuristic tuning in the problem of fast-changing atmospheric patterns. Similarly, a geographically aware CNN-LSTM-KAN (integrating climatic and topographic differentiation) model was proposed in Hu et al. [22], and it was proven to achieve significant improvement in reducing RMSE (23.6-59.6%) and R^2 of 0.92-0.99 in five geographically and climatically varied Chinese cities, compared to standard LSTM and CNN-LSTM baselines. In addition to this, Utku et al. [23] proposed a lightweight CNN-RNN hybrid, which was evaluated in three cities, viz., India, Milan, and Frankfurt, and outperformed several ML and DL baselines.

Although any emission-regime shift was not specifically studied, because the model was shown to perform consistently in diverse locations, some generalizations may be feasible. Collectively, these advances in deep learning indicate huge progress on the modeling of non-stationary pollutant behavior and complex spatio-temporal dependencies. However, even though they are predictive, these kinds of architectures are purely data-driven and do not account for atmospheric physics, pollutant transformation rules, or AQI formulation principles. As a consequence of this, their outputs may violate physical consistency under unseen conditions or regime shifts, which highlights the need for physics-informed or scientific machine learning methods that integrate data and domain knowledge.

To mitigate these limitations, physics-based solutions were proposed in the form of physics-informed neural networks (PINNs) to impose physical consistency on machine learning and deep learning models. Instead of using only historical correlation, PINNs take the form of using governing equations and domain constraints in the learning process [6]. Building upon this base, in the last few years, applications of physics-informed and scientific machine learning methods in air quality problems started to be published. For instance, Shi et al. [24] proposed Phy-APMR, a model that couples a neural network with a groundspeed definition primarily based on a practical pollutant transport beforehand to rebuild fine-grained concentration declaration from sparse mobile sensors. Their framework, in comparison, had about 15% fewer reconstruction errors and up to 84% better training time than state-of-the-art baselines, providing one proof of concept to explain the importance of incorporating physical propagation constraints under data sparsity. Similarly, Li et al. [25] proposed the knowledge-informed deep learning approach for joint pollution predictions to decrease the biases and enhance the generalization; even though it does not consider explicit transport equations, the physical underpinning of the approach is still limited related to unusual atmospheric regimes. In parallel, Chandrashekar et al. [2] published a hybrid model called AirSense-X consisting of PINN-inspired and XAI-based ideas that had an accuracy of roughly 98% in AQI classification. Yet the lack of explicit physical equations and the focus on the categorical prediction of AQI rather than on the prediction of future AQI concentrations, raises the question of how directly 'physics-informed' the model really is and whether it'll be able to generalize under changing atmospheric conditions.

Overall, there has been no previous study to systematically benchmark the effect of the integration of simple AQI formulation physics in multiple model families, pollutants $PM_{2.5}$ and O_3 , and temporal lag structures. This gap underpins the present study, which evaluates the influence of incorporating EPA-style piecewise AQI mapping to diverse ML and DL architectures towards predictive performance, robustness, and physical consistency at lag-1, lag-7, lag-14, and lag-30 based forecasting scenarios. Through this benchmarking analysis, the study attempts to understand the characteristics of when and how the physics-based constraints have added significant value to air quality prediction, as well as whether this is the same for various pollutants and model complexities. Table 1 is a summary of most

representative ML, DL, hybrid, and physics-informed methods adopted in recent air quality prediction research, which encompasses most of the architectures, performance, and limitations.

Related Study	Model Architecture	Datasets	Task	Results	Tentative Research Gap
Li et al. [17]	Random Forest regression	Huaihai Economic Zone, China (2000–2020)	Daily PM _{2.5} estimation	$R^2 = 0.85$, RMSE = 14.63 $\mu\text{g}/\text{m}^3$, MAE = 10.03 $\mu\text{g}/\text{m}^3$	No physics; cannot capture long-range temporal interactions.
Ravindiran et al. [18]	CatBoost / ensemble ML	Visakhapatnam, India (2017–2022)	AQI forecasting	$R^2 \approx 0.9998$, RMSE ≈ 0.76	Extremely high fit; may overfit; relies entirely on historical correlations.
Yenkikar et al. [5]	Random Forest + ARIMA residual modeling	India (station-level data)	AQI forecasting	MSE ≈ 508.46 ; $R^2 \approx 0.94$	No DL; limited temporal modeling; no physical knowledge.
Sarkar et al. [19]	LSTM–GRU hybrid	Delhi, India	AQI prediction	MAE = 36.11; $R^2 = 0.84$	Single-city; no spatial modeling; fully data-driven.
Elbaz et al. [20]	3D-CNN + GRU + Attention	China (regional / national)	Multi-horizon PM _{2.5} forecasting	Outperformed 2D-CNN, 3D-CNN, GRU baselines in RMSE / MAE	Needs large image + met datasets; computationally heavy; no explicit physics.
Hu et al. [22]	CNN–LSTM–KAN hybrid	Five Chinese cities	AQI / pollutant forecasting	RMSE reduced 23.6–59.6%; $R^2 = 0.92–0.99$	High complexity; generalization beyond studied cities untested.
Shi et al. [24]	Phy-APMR (NN + pollutant-transport PDE + ASUS)	Multiple Chinese cities	Fine-grained pollution map reconstruction	$\sim 15\%$ lower error; $\sim 84\%$ faster convergence	Requires mobile sensors; focuses on mapping, not forecasting; PDE assumptions limit transferability.
Chandrashekar et al. [2]	PINN + XAI (AQI classification)	India (multi-city)	AQI classification	Accuracy $\approx 98\%$; precision 97%; recall 95%; F1 = 0.96	No explicit PDE physics; classification only, not forecasting.

Table 1: Comparison of major ML, DL, hybrid, and physics-informed approaches for air-quality prediction and forecasting.

3 Datasets Description

3.1 Data Collection

In this research study, a publicly available air quality data set is collected from the United States Environmental Protection Agency (EPA) through the outdoor daily air quality data portal [26]. The dataset includes three consecutive years of observations, 2022, 2023, and 2024, for benchmarking the physics impact on AQI prediction. To analyze the air quality of the highly polluted zone in Texas, Dallas County, has been selected, and data has been collected from a total of three stations (Convention Center, Dallas Hinton, and Dallas Bexar Street). For each year, we downloaded the daily records for fine particulate matter Particulate Matters (PM_{2.5}) and Ozone (O₃), and the Air Quality Index (AQI) from all EPA monitoring stations operating within the Dallas county.

3.2 Data Aggregation

Each raw yearly dataset contains daily pollutant measurements collected independently at multiple monitoring sites. To obtain a representative city-level estimate of daily air quality, all station observations for the same day were averaged. This produced a single time-series file per year containing the daily mean PM_{2.5} concentration and the corresponding daily mean AQI value. The three yearly files were then merged into one continuous multi-year dataset covering the period January 2022 to December 2024. Similarly, we collected data for the ozone (O₃) and then merged it into one continuous multi-year dataset covering the period January 2022 to December 2024 as well. Before analysis, the merged datasets were cleaned by converting date formats to a unified structure, removing incomplete records, and ensuring consistent column naming. This resulted in a high-quality daily datasets for PM_{2.5} and O₃ containing three primary variables: DATE, Daily_Mean_PM or Daily_Mean_Ozone, and Daily_AQI_Value. Table 2 summarizes the base PM_{2.5}

and O_3 datasets used to construct multi-horizon AQI targets. The datasets contain 1094 and 1091 daily observations, respectively, covering the period 2022–2024. Each record includes the daily mean pollutant concentration and the corresponding EPA AQI value. The datasets exhibit substantial variability in both pollutant levels and AQI, providing a robust foundation for deep learning–based forecasting experiments.

Table 2: Summary statistics of the base $PM_{2.5}$ and O_3 datasets used for constructing multi-horizon AQI targets.

Statistic	$PM_{2.5}$ Dataset (2022–2024)	O_3 Dataset (2022–2024)
Number of daily records	1094	1091
AQI (min)	6.00	2.67
AQI (max)	124.00	168.33
AQI (mean \pm std)	46.18 \pm 14.90	41.82 \pm 20.78
Pollutant value (min)	0.45 $\mu\text{g}/\text{m}^3$	0.0027 ppm
Pollutant value (max)	44.85 $\mu\text{g}/\text{m}^3$	0.0927 ppm
Pollutant (mean \pm std)	9.62 \pm 4.90 $\mu\text{g}/\text{m}^3$	0.0415 \pm 0.0138 ppm

3.3 Lag-Wise Dataset Transformation for Multi-Horizon Forecasting

For benchmarking for AQI forecasting, the individual multi-year datasets were further converted into a lag-based prediction structure. In this formulation the target variable is the future value of the AQI, shifted up by a certain number of days. The forecasting horizon is chosen to be $LAG = 1$, $LAG = 7$, $LAG = 14$, and $LAG = 30$, and the dataset matches the pollutant values measured on each day with the AQI value of the following lag days. This transformation adds a new variable, $AQI_Targeted_Value_LAG_L$, that is the value of AQI L days ahead of each observation. Rows in which the future AQI values are not valid (including the last L days of the dataset) were dropped in order to maintain dataset completeness. Each lag-specific dataset, therefore, includes well-aligned feature-target pairs comprising the current day’s pollutant concentration ($PM_{2.5}$ or O_3), the current day’s daily AQI value, and the AQI value L days in the future target. A total of four datasets have been generated for $PM_{2.5}$ and lag sizes of 1, 7, 14, and 30, and another four datasets have been generated for O_3 and the same lag values. Dataset preparation techniques are shown in the Algorithm 1. This lag-wise technique allows for rigorous forecasting experiments for a variety of time horizons and allows for the evaluation of physical influences on the predictability of AQIs. The resulting processed datasets are clean and temporally consistent and appropriate for machine learning and physics-informed modeling as the basis for the predictive analysis performed in this study.

To illustrate the structure of the lag-wise datasets used for forecasting, Tables 3 present sample records for $PM_{2.5}$ and O_3 , respectively. It lists the current-day features, daily mean pollutant concentration and corresponding AQI value alongside four future AQI targets generated using different forecasting horizons ($LAG = 1$, 7, 14, and 30 days). These examples demonstrate how each observation is aligned with multiple future AQI values, enabling the development and evaluation of multi-horizon air-quality prediction models for both $PM_{2.5}$ and O_3 .

Table 3: First 10 samples of the lag-wise $PM_{2.5}$ and O_3 datasets across multiple forecasting horizons.

DATE	$PM_{2.5}$ Data						O_3 Data					
	$PM_{2.5}$	AQI	L1	L7	L14	L30	O_3	AQI	L1	L7	L14	L30
01-01-22	6.10	34.00	26.00	61.00	27.00	19.00	0.0250	23.00	30.33	15.67	26.67	31.33
02-01-22	4.60	26.00	52.00	23.00	55.00	24.50	0.0323	30.33	27.67	24.33	29.00	33.00
03-01-22	9.60	52.00	29.00	31.00	64.25	21.00	0.0297	27.67	33.33	22.00	28.67	27.67
04-01-22	5.30	29.00	32.67	49.00	37.00	6.00	0.0360	33.33	30.67	26.67	40.67	28.67
05-01-22	5.90	32.67	39.00	35.00	44.00	41.33	0.0330	30.67	23.00	29.67	23.33	34.00
06-01-22	7.10	39.00	42.00	43.00	9.00	64.00	0.0250	23.00	23.33	28.67	26.00	34.00
07-01-22	7.50	42.00	61.00	52.67	17.00	32.00	0.0253	23.33	15.67	41.33	26.50	36.33
08-01-22	14.47	61.00	23.00	27.00	55.00	42.33	0.0167	15.67	24.33	26.67	25.00	30.33
09-01-22	4.20	23.00	31.00	55.00	50.33	25.50	0.0263	24.33	22.00	29.00	33.50	34.33
10-01-22	5.60	31.00	49.00	64.25	26.00	50.00	0.0237	22.00	26.67	28.67	18.00	32.33

Algorithm 1 Construction of Multi-Year Lag-based AQI Prediction Dataset

Input: Years $\mathcal{Y} = \{2022, 2023, 2024\}$; Collect EPA Daily Data $\{\text{file}_y : y \in \mathcal{Y}\}$; forecast horizon $LAG \in \mathbb{N}$

Output: Lag-wise dataset $\mathcal{D}^{(LAG)}$ for Lag-day-ahead AQI forecasting

```
1: Stage 1: Multi-Year Station-Averaged EPA Dataset
2: Initialize list  $\mathcal{D}_{avg} \leftarrow []$ 
3: for each year  $y \in \mathcal{Y}$  do
4:    $D_y \leftarrow \text{LoadCSV}(\text{file}_y)$ 
5:   Convert  $D_y[\text{Date}]$  to datetime
6:    $D_y \leftarrow \text{DropNA}(D_y, \{\text{Date}, \text{Conc}, \text{AQI}\})$ 
7:    $D_y \leftarrow \text{SortByDate}(D_y)$ 
8:   for each unique date  $t$  in  $D_y$  do
9:      $\bar{c}_y(t) \leftarrow \text{Mean}\{r.\text{Conc} : r.\text{Date} = t\}$ 
10:     $\bar{a}_y(t) \leftarrow \text{Mean}\{r.\text{AQI} : r.\text{Date} = t\}$ 
11:   end for
12:    $D_y^{avg} \leftarrow \{(t, \bar{c}_y(t), \bar{a}_y(t))\}_t$ 
13:   Append  $D_y^{avg}$  to list  $\mathcal{D}_{avg}$ 
14: end for
15:  $D^{multi} \leftarrow \text{Concat}(\mathcal{D}_{avg})$ 

16: Stage 2: Lag-based Dataset Preparation
17: Load combined CSV into data frame  $df$ 
18:  $df \leftarrow \text{ResetIndex}(df)$ 
19:  $data \leftarrow df[\text{DATE}, \text{Daily\_Mean\_PM}, \text{Daily\_AQI\_Value}]$ 
20: Choose forecast horizon  $LAG \geq 1$ 
21: for  $i = 1$  to number of rows in  $data$  do
22:   if  $i + LAG \leq$  number of rows then
23:      $\text{AQI\_Targeted\_Value\_LAG\_L}[i] \leftarrow \text{Daily\_AQI\_Value}[i + LAG]$ 
24:   else
25:      $\text{AQI\_Targeted\_Value\_LAG\_L}[i] \leftarrow \text{NaN}$ 
26:   end if
27: end for
28: Append column  $\text{AQI\_Targeted\_Value\_LAG\_L}$  to  $data$ 
29:  $\mathcal{D}^{(LAG)} \leftarrow data[\text{DATE}, \text{Daily\_Mean\_PM}, \text{Daily\_AQI\_Value}, \text{AQI\_Targeted\_Value\_LAG\_L}]$ 
30: return  $\mathcal{D}^{(LAG)}$ 
```

3.4 Data Pre-processing

To fit the data into the different targeted model, rows containing missing features or missing future-day targets were validated to ensure complete training examples. After constructing these final lag-wise datasets, all samples were split chronologically using an 80–20 ratio, where the first portion formed the training set and the remaining future portion formed the test set. This prevented information from future days from leaking into the training stage and ensured that all models were evaluated under realistic forecasting conditions.

As, different model families required slightly different preparation steps. Linear regression used the raw, unscaled pollutant and AQI values. SARIMAX used the AQI series as the main time-series input and included a one-day-lagged pollutant value as an exogenous regressor; the series was set to daily frequency, forward-filled when necessary, and split without scaling. In contrast, MLP and MLP+Physics models applied standardization to input features using statistics computed only from the training set, while keeping AQI targets in their real units. LSTM and LSTM+Physics models used min-max normalization for both inputs and targets to support stable gradient-based training; after prediction, AQI outputs were inverse-transformed back to real physical units. This unified and carefully controlled preprocessing pipeline ensured consistency across model families, avoided data leakage, and preserved the interpretability of AQI predictions.

4 Methodology

A structured scientific machine learning workflow has been designed and followed to integrate the environment data processing, create supervised multi-horizon datasets for the forecast, develop models for benchmarking, integrate

physics into the model learning, and perform a detailed comparative evaluation for benchmarking the air quality index for Dallas County. The overall conceptual model is that starting from raw pollutant and AQI measurements from EPA monitoring stations, the data is passed through a series of data preparation, feature engineering, model training, and performance benchmarking steps, which are reflected in the workflow diagram in Figure 1.

The required dataset has been assembled and preprocessed using the procedure described in Algorithm 1 in Section 3. This pre-processed data goes into a consolidation modeling stage where classical machine-learning models, deep-learning architectures, and physics-guided models are applied to the same lag-wise datasets. The physics guidance includes the use of EPA’s AQI formulation, which relates the concentration of pollutant to the AQI using breakpoint-based piecewise rules. Then, the structured workflow provides a consistent and reproducible basis, with a scientific underpinning, for assessing AQI forecasting models. By applying all the lag-wise datasets separately to several model families such as linear regression, SARIMA, MLP, and LSTM, and finally then the MLP+Physics and LSTM+Physics frameworks, a fair assessment of the role of model complexity and domain knowledge in predictive performance is made possible. Embedding physics-guided knowledge constraints provides a guarantee that not only the deep learning models optimized by tuning their hyperparameters, but also that they are guided to physically meaningful behavior.

4.1 Baseline Statistical and Machine-Learning Models

4.1.1 Linear Regression

One of the most commonly used statistical learning models is linear regression to represent the relationships between predictors and a continuous response variable, originating from the classical least-squares framework[27, 28]. As a baseline for the AQI forecasting, a linear regression model has been used and applied to the PM_{2.5} and O₃ datasets among all the forecasting horizons with LAG 1, 7, 14, and 30, respectively. The model assumes a linear relationship between the current-day pollutant level and AQI and the next-day AQI target and provides an interpretable benchmark for comparing the performance of more advanced time-series and deep-learning models. For each dataset, the features consisted of the current day’s pollutant concentration and AQI value, while the target variable corresponded to the AQI value at the specified future horizon. To validate the effect of the normalization, both scaling and no scaling with StandardScaler are performed. When scaling was applied, the transformation parameters were learned exclusively from the training portion of the data and applied consistently to the test set to prevent information leakage. The linear regression model follows the standard Ordinary Least Squares formulation, where the relationship between inputs and the predicted AQI is modeled as

$$\hat{y} = \beta_0 + \beta_1 \text{Daily_Mean_Pollutant}(t) + \beta_2 \text{Daily_AQI_Value}(t), \quad (1)$$

and the coefficients β_0 , β_1 , and β_2 are estimated by minimizing the residual sum of squares. This simple architecture provides a transparent, interpretable mapping from current-day conditions to the future AQI. This baseline allows a clear comparison between simple data-driven learning and more complex architectures such as SARIMA, MLP, LSTM, and the physics-guided PINN variants.

4.1.2 SARIMAX

The Seasonal AutoRegressive Integrated Moving Average with eXogenous regressors (SARIMAX) is a model extending the classical Box-Jenkins ARIMA and SARIMA models [29] that adds external predictor(s) to the system. It permitted capturing both internal temporal structure and exogenous influences in time series forecasting and was fast-used in weather forecasting as well [30, 31, 32]. In order to focus on both short-term autoregressive nature and seasonal patterns from the datasets, the SARIMAX model is trained and tested on all lag-wise datasets, which will ensure the primary classical time series baseline for benchmarking. A fixed configuration with non-seasonal order and seasonal order is employed, which reflects both short-term AQI dynamics as well as weekly seasonal patterns for AQI and is applied the same way for all LAG 1, 7, 14, and 30 datasets and appropriately aligned before training. For each lag-wise dataset, the current day AQI series is taken as an endogenous variable, whereas the previous day’s pollutant concentration is added as a lagged exogenous regressor. This enables the model to reflect the internal temporal characteristics of AQI and the external influence of pollutant fluctuation with time. StandardScaler is always fitted only on the training set of each dataset, to prevent information leakage before fitting the test set using the same parameters. The model is implemented using the Statsmodels SARIMAX framework and is fitted using maximum likelihood estimation by CPU resources because GPU acceleration is not providing extra benefits for this class of statistical models. Separate experiments are carried out for each forecasting horizon, which makes it possible to assess the variation in difficulty of prediction for the short- and medium-term horizons. The SARIMAX architecture combines the non-seasonal ARIMA components with a seasonal ARIMA structure and an exogenous pollutant regressor. In this setup, the AQI value at time t is influenced by its own past values, past error terms, weekly seasonal dependencies, and the lagged pollutant concentration. The

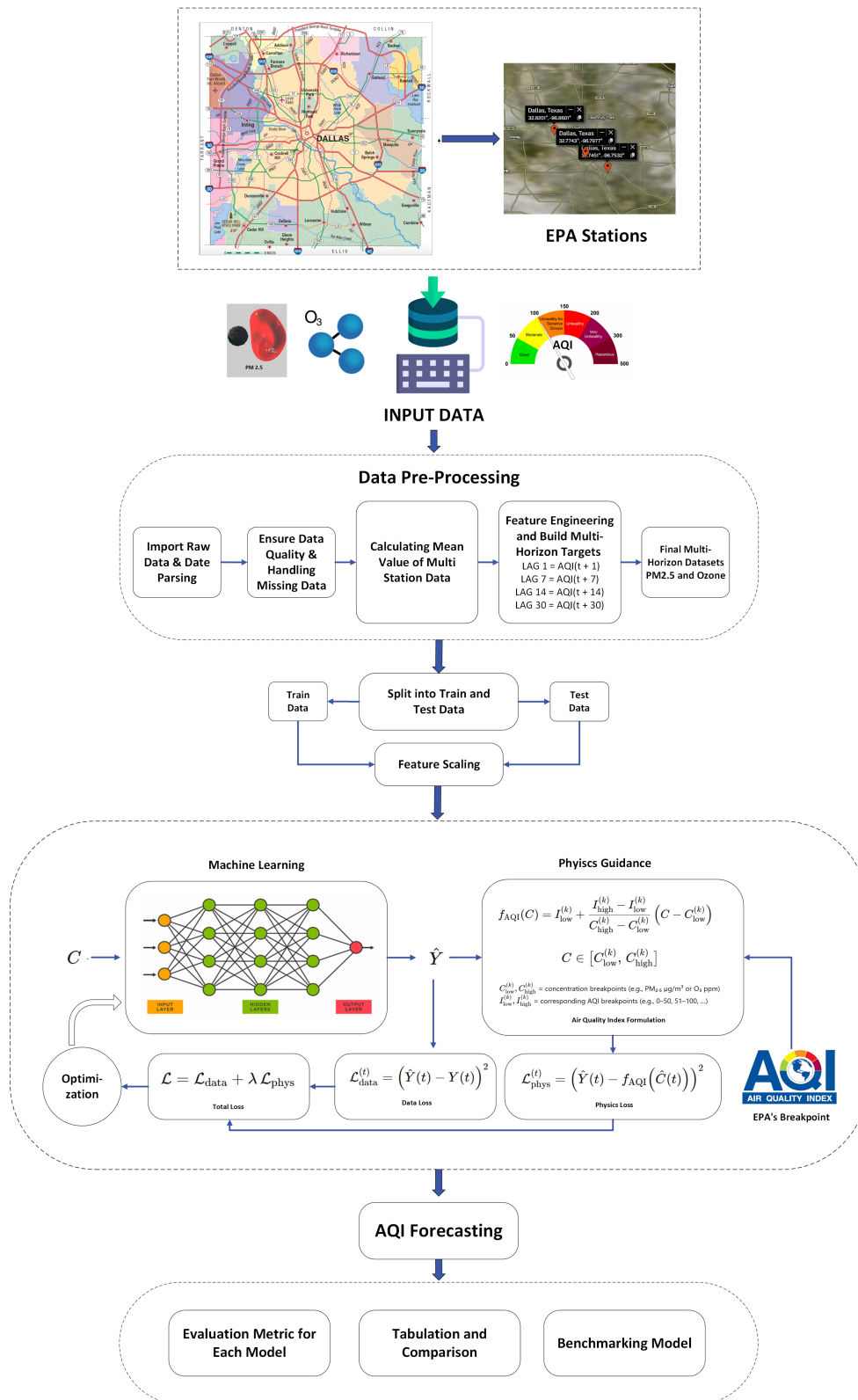


Figure 1: Proposed conceptual model for Physics Guided Scientific Machine Learning for Air Quality Index Forecasting.

Algorithm 2 Generalized Multi-Model Lag-Wise AQI Forecasting with and without Physics Guidance

Input: Lag-wise datasets $\mathcal{D}^{(p,LAG)}$ constructed using Algorithm 1 for pollutants $p \in \{\text{PM}_{2.5}, \text{O}_3\}$ and horizons $LAG \in \{1, 7, 14, 30\}$;

Model set $\mathcal{M} = \{\text{LR}, \text{SARIMA}, \text{MLP}, \text{MLP} + \text{Phys}, \text{LSTM}, \text{LSTM} + \text{Phys}\}$;

Train-test split ratio α (e.g., 0.8); EPA AQI breakpoint tables \mathcal{B} ; loss weights $\lambda_{\text{data}}, \lambda_{\text{phys}}$.

Output: Trained models and evaluation metrics (MAE, RMSE, R^2) for each (p, LAG, m) .

1: **Stage 1: Dataset Pre-Processing**

2: Use Algorithm 1 to construct the LAG-wise dataset $\mathcal{D}^{(p,LAG)}$.

3: Split each $\mathcal{D}^{(p,LAG)}$ chronologically into training (first α) and testing (remaining $1 - \alpha$).

4: Fit a scaler on training features/targets only (for ML/DL models) and transform both sets. SARIMA uses the raw AQI series without scaling.

5: **Stage 2: Model Definition**

6: **for** each model type $m \in \mathcal{M}$ **do**

7: **if** $m = \text{LR}$ **then**

8: Define linear regression model $y = \beta_0 + \beta_1 \text{Daily_Mean}_p + \beta_2 \text{AQI}_t$.

9: **else if** $m = \text{SARIMA}$ **then**

10: Define SARIMA(p, d, q)(P, D, Q)_s on the univariate AQI series.

11: **else if** $m = \text{MLP}$ or $\text{MLP} + \text{Phys}$ **then**

12: Define a feed-forward MLP mapping $\mathbf{x}_t \mapsto \hat{y}_t$.

13: **else if** $m = \text{LSTM}$ or $\text{LSTM} + \text{Phys}$ **then**

14: Define a one-to-one LSTM-based model (Algorithm 3) mapping $[\text{Daily_Mean}_p(t), \text{AQI}_t] \mapsto \hat{y}_t$.

15: **end if**

16: **end for**

17: **Stage 3: Physics Guided AQI formulation**

18: Define PhysicsAQI(c_t, \mathcal{B}) using the EPA piecewise linear AQI formula: $\text{AQI}_t^{\text{phys}} = (I_{\text{hi}} - I_{\text{lo}}) \frac{(c_t - C_{\text{lo}})}{(C_{\text{hi}} - C_{\text{lo}})} + I_{\text{lo}}$.

19: Return $\text{AQI}_t^{\text{phys}}$ (scaled if required).

20: **Stage 4: Training Loop for Each Model and Dataset**

21: **for** each (p, LAG) **do**

22: **for** each model type $m \in \mathcal{M}$ **do**

23: **if** $m = \text{SARIMA}$ **then**

24: Fit SARIMA on the raw training AQI series and skip gradient-based training.

25: **else**

26: **for** epoch = 1 to max_epochs **do**

27: Compute predictions on training data and evaluate data loss.

28: **if** m is physics-informed **then**

29: Compute physics-based AQI and physics loss.

30: Total loss: $\mathcal{L} = \lambda_{\text{data}} \mathcal{L}_{\text{data}} + \lambda_{\text{phys}} \mathcal{L}_{\text{phys}}$.

31: **else**

32: $\mathcal{L} = \mathcal{L}_{\text{data}}$.

33: **end if**

34: Backpropagate \mathcal{L} and update model parameters.

35: **end for**

36: **end if**

37: **end for**

38: **end for**

39: **Stage 5: Testing and Evaluation**

40: **for** each (p, LAG) and model $m \in \mathcal{M}$ **do**

41: Generate predictions on train and test sets.

42: **if** $m \neq \text{SARIMA}$ **then**

43: Apply inverse scaling to recover predictions and targets in real AQI units.

44: **end if**

45: Compute MAE, RMSE, and R^2 in real units and save in benchmarking table.

46: **end for**

general model formulation is expressed as:

$$y_t = \phi_1 y_{t-1} + \theta_1 \varepsilon_{t-1} + \Phi_1 y_{t-7} + \Theta_1 \varepsilon_{t-7} + \beta x_{t-1} + \varepsilon_t, \quad (2)$$

where y_t denotes the AQI at time t , x_{t-1} is the pollutant concentration from the previous day, and ε_t is the model residual. This formulation captures both short-term dependencies and recurring weekly seasonal effects in AQI while integrating pollutant-driven variations. This SARIMAX configuration therefore provides a consistent and interpretable classical baseline against which the performance of the MLP, LSTM, and physics-guided PINN models can be systematically compared.

4.2 Deep-Learning Models for AQI Forecasting

4.2.1 Multilayer Perceptron (MLP) Model

Multilayer Perceptrons (MLPs) [33] is among the first known and very popular neural network architectures for nonlinear function approximation, and these were successfully applied in weather and environmental forecasting problems since they have the capacity to model complex relationships between atmospheric variables and future weather conditions [34, 35]. The MLP model is utilized as a nonlinear supervised baseline in between the simple linear regression and more complicated models (LSTM and physics-guided models). For each pollutant ($\text{PM}_{2.5}$ and O_3) and each forecasting horizon (LAG 1, 7, 14, and 30), the model is trained using the lag-wise datasets as mentioned earlier. In each of these cases, the input features are the concentration of pollutants and the AQI value of the current day, and the target is the AQI value at the selected lag in the future. The data are then divided chronologically with an 80%–20% train-test division with no shuffling to maintain order. StandardScaler is applied for the input features, and these parameters are learned from the training part; hence, these parameters are used for transforming the test set, whereas the targeted AQI is kept in its original value.

The MLP design is built using PyTorch as a fully connected feedforward network with two input neurons (for pollutant and AQI) and two hidden layers with 64 and 32 neurons, respectively. Each hidden layer uses ReLU activation to capture nonlinear interactions. The forward propagation of the MLP can be expressed as:

$$\hat{y}_{t+L} = W_3 \sigma(W_2 \sigma(W_1 x_t + b_1) + b_2) + b_3, \quad (3)$$

where $x_t = [\text{PM}_{2.5}(t)/\text{O}_3(t), \text{AQI}(t)]^\top$ is the two-dimensional input vector, W_1 , W_2 , and W_3 denote the learnable weight matrices, b_1 , b_2 , and b_3 are the corresponding biases, and $\sigma(\cdot)$ represents the ReLU activation function. A last linear output neuron makes a single scalar prediction for the AQI value in the future. The AdamW optimizer with a learning rate of 0.001 and a mean squared error (MSE) loss calculated directly in AQI units is used to train the model across a set number of epochs. MAE, RMSE, and R^2 evaluation metrics are used to measure the model’s performance on a held-out test set after training. Such MLP model provided us a data-driven benchmark which is nonlinear and that can be used to compare with the other ML/DL models and their physics-informed versions.

4.2.2 Long Short-Term Memory (LSTM) Model

Long Short-Term Memory (LSTM) [36] works on sequential data and is very effective for predicting long-range time series dependencies, which use RNN to memorize the information from earlier events and make decisions accordingly [37]. LSTM is used in weather forecasting and air quality data analysis for its effective decision-making on time-series data [38, 39]. A LSTM network has been developed as a nonlinear sequence-based baseline to capture temporal dependencies in AQI evolution. For each pollutant ($\text{PM}_{2.5}$ and O_3) and forecasting horizon (LAG 1, 7, 14, and 30), the model is trained on the same lag-wise datasets used for the MLP and statistical baselines. Each lag-wise dataset provides two input features: the current day’s pollutant concentration and AQI value along with the corresponding future AQI value at the selected forecasting horizon. An 80%–20% chronological split is used to preserve forecasting realism. To ensure consistent preprocessing, min-max normalization in the range $[-1, 1]$ is fitted only on the training portion of each dataset using all three relevant columns (pollutant, AQI, and future AQI). The same transformation is then applied to the test set, preventing any information leakage. For the model architecture, the sequence length is settled to $T = 1$ along with two features, $F = 2$, that produced tensors of shape that are perfect for building an LSTM model.

The model is built with PyTorch, which consists of two stacked unidirectional LSTM layers that have 32 hidden units individually and are then followed by deep, fully connected layers of 128, 64, and 32 neurons with activation functions and dropout regularization. The forward computation of each LSTM cell follows the standard gated formulation:

$$\begin{aligned}
i_t &= \sigma(W_i x_t + U_i h_{t-1} + b_i), \\
f_t &= \sigma(W_f x_t + U_f h_{t-1} + b_f), \\
o_t &= \sigma(W_o x_t + U_o h_{t-1} + b_o), \\
\tilde{c}_t &= \tanh(W_c x_t + U_c h_{t-1} + b_c), \\
c_t &= f_t \odot c_{t-1} + i_t \odot \tilde{c}_t, \\
h_t &= o_t \odot \tanh(c_t),
\end{aligned} \tag{4}$$

where $x_t \in \mathbb{R}^2$ contains the current pollutant level and AQI value, i_t , f_t , and o_t denote the input, forget, and output gates, c_t is the cell state, and h_t is the hidden state passed to subsequent layers. Then a final linear neuron provided the final output in scaled units. The model is optimized by using Adam and a learning rate of 0.0001, followed by MSE loss. The learning rate is adjusted by a ReduceLROnPlateau scheduler when validation loss plateaus, and we used early stopping with a patience of 20 epochs to ensure the generalization. After training, predictions are inverse-transformed back to real AQI units, and evaluation is performed using R^2 , MAE, and RMSE. This LSTM baseline provides a sequence-oriented deep-learning benchmark for comparison with the MLP and the physics-informed LSTM variants.

4.3 Proposed Physics-Informed Model for AQI Prediction

A physics-guided machine learning model helps the model to learn more about the domain knowledge and incorporate it into the overall learning process [6]. To analyze and benchmark the knowledge guidance on AQI prediction, a physics-guided model is proposed in this research. We implemented and applied the domain knowledge of the AQI calculation directly to the ML/DL model and proposed one hybrid model with MLP+Physics and another hybrid deep learning model, LSTM+Physics. Domain knowledge information for calculating the AQI equation provided by the U.S. EPA has been applied to our developed neural network [26]. It is worth mentioning that our baseline models (LR, SARIMAX, MLP, and LSTM) are completely dependent on the statistical data and the relationship between PM and ozone concentrations, as well as on future AQI values. However, in this research, the proposed MLP+Physics and LSTM+Physics models provided the domain knowledge for AQI calculation that powered the learning function to stay more consistent. The AQI is defined using a piecewise linear function, in which each pollutant concentration interval $[C_{\text{low}}^{(k)}, C_{\text{high}}^{(k)}]$ corresponds to an AQI interval $[I_{\text{low}}^{(k)}, I_{\text{high}}^{(k)}]$. For any concentration value C_i that falls within the k -th EPA breakpoint range, the AQI is computed as:

$$f_{\text{AQI}}(C_i) = I_{\text{low}}^{(k)} + \frac{I_{\text{high}}^{(k)} - I_{\text{low}}^{(k)}}{C_{\text{high}}^{(k)} - C_{\text{low}}^{(k)}} (C_i - C_{\text{low}}^{(k)}), \quad C_i \in [C_{\text{low}}^{(k)}, C_{\text{high}}^{(k)}]. \tag{5}$$

This formulation is applied using the full EPA breakpoint tables [40] for both $\text{PM}_{2.5}$ and O_3 , covering all AQI categories from ‘‘Good’’ to ‘‘Hazardous,’’ and the computed AQI values are capped at the EPA maximum of 500. The output of this function serves as a physics-based AQI reference that guides the neural models toward pollutant–AQI relationships that adhere to established atmospheric behavior.

To embed this physical knowledge into the learning process, the supervised data loss is combined with a physics-based consistency loss. The standard data-driven loss is defined as:

$$\mathcal{L}_{\text{data}} = \frac{1}{N} \sum_{i=1}^N (\hat{y}_i - y_i)^2, \tag{6}$$

where \hat{y}_i is the model prediction and y_i is the true AQI value.

The physics loss penalizes deviations between the model prediction and the EPA-derived AQI computed from pollutant concentrations:

$$\mathcal{L}_{\text{phys}} = \frac{1}{N} \sum_{i=1}^N (\hat{y}_i - f_{\text{AQI}}(C_i))^2. \tag{7}$$

The total loss combines these two terms using a weighted formulation:

$$\mathcal{L}_{\text{total}} = \lambda_{\text{data}} \mathcal{L}_{\text{data}} + \lambda_{\text{phys}} \mathcal{L}_{\text{phys}}, \tag{8}$$

where λ_{data} and λ_{phys} control the balance between empirical data fitting and adherence to physically grounded AQI behavior. By adjusting these weights, the framework spans purely data-driven learning ($\lambda_{\text{phys}} = 0$) to fully physics-constrained modeling ($\lambda_{\text{data}} = 0$). This unified physics-informed formulation is applied consistently across both the MLP+Physics and LSTM+Physics architectures, enabling systematic evaluation of physics-guided deep learning for AQI forecasting across pollutants and multi-horizon settings.

4.3.1 MLP+Physics

The proposed MLP+Physics model incorporates the EPA AQI formulation for both $\text{PM}_{2.5}$ and O_3 , and each pollutant-specific model is trained separately following the same procedure used for the baseline MLP. The physics formula is imposed directly within the training loss function. The model architecture mirrors the baseline design: the input vector x_t contains two features, the current day’s pollutant concentration and AQI value that scaled using a `StandardScaler` fitted strictly on the training portion of each lag-wise dataset. The network contains two fully connected hidden layers with 64 and 32 neurons, respectively, each followed by a ReLU activation, and a final linear output neuron that produces a single predicted AQI value in real AQI units.

During training, the forward pass produces the model prediction \hat{y}_i , while the pollutant concentration C_i is simultaneously passed through the EPA breakpoint-based AQI computation to generate the physics-derived reference value $f_{\text{AQI}}(C_i)$ defined in Equation (5). The data-driven loss follows the form given in Equation (6), and the physics-based loss follows Equation (7). These two components are combined using scalar weights λ_{data} and λ_{phys} as defined in the total loss expression in Equation (8). Optimization is performed using the AdamW optimizer with a learning rate of 0.001 over a fixed number of epochs. This hybrid design enforces simultaneous learning from empirical data and established pollutant–AQI relationships. Because the MLP architecture remains constant across horizons, this physics-guided model provides a consistent nonlinear benchmark for assessing the influence of domain knowledge on prediction performance across pollutants and forecasting horizons.

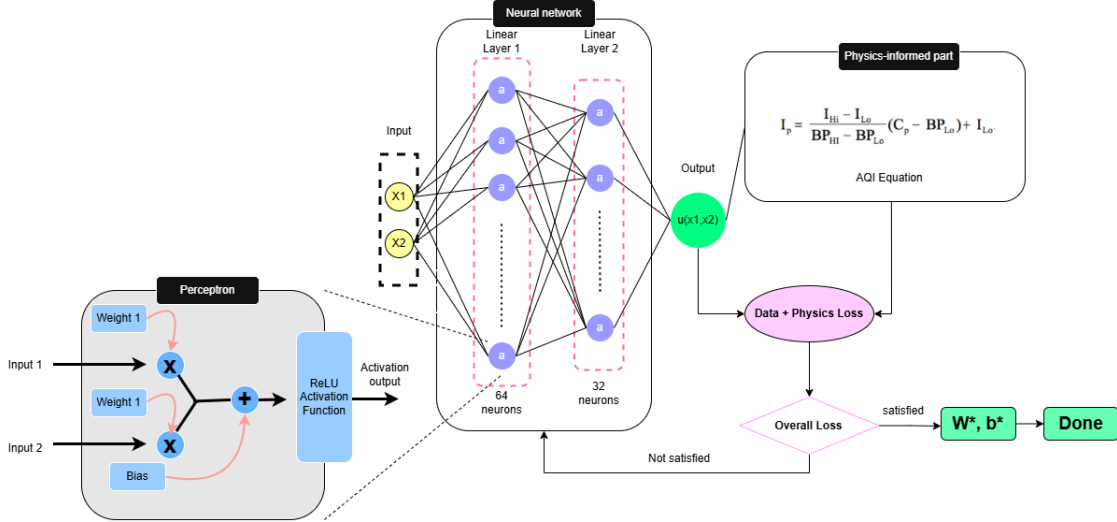


Figure 2: Architecture of the MLP+Physics Model.

4.3.2 LSTM + Physics Integration

The proposed LSTM+Physics model has been implemented by using the same baseline LSTM model architecture and integrating Equation (5) into the learning part of the model. This model is trained individually for $\text{PM}_{2.5}$ and O_3 with the lag-wise datasets of the multi-horizons. The input sequence is designed by the current day’s pollutant concentration along with the AQI value. The target variable is defined as the AQI from the future lag days within the forecasting horizon. The sequence data is normalized using a Min–Max scaler fitted strictly on the training portion of each dataset. First of all, two stacked unidirectional LSTM layers have been used with 32 hidden layers for each, and a multilayer fully connected layer is being followed with 128, 64, and 32 neurons and activated by ReLU, and then dropout regularization is applied. Finally, a linear neuron outputs the predicted AQI value in the scaled domain that is inverse-transformed later to real AQI units for evaluation.

To train the model effectively, a forward pass created the prediction \hat{y}_i of the model for every sample input, and the respective pollutant concentration C_i is then provided to the AQI function $f_{\text{AQI}}(C_i)$ defined in Equation (5), that helps

and provides the domain knowledge to the training process. Data-driven loss has been calculated by using the MSE formula described in Equation (6), and the physics loss has been calculated from Equation (7). Finally, total loss has been calculated from the data loss and physics loss by the equation (8). Overall, this process ensures a balance between learning and physical consistency in order to accurately detect the AQI based on pollutant concentration.

The model is optimized using the Adam optimizer, which has a learning rate of 0.0001. A ReduceLROnPlateau scheduler adjusts the learning rate when the validation loss reaches saturation, and early pausing with a 20-epoch patience is employed to promote generalization. By including the physics-based AQI constraints into the sequence-learning architecture, the LSTM+Physics model enforces domain-aware temporal reasoning. This strengthens the benchmark for assessing how physical knowledge enhances AQI forecasting over many horizons and contaminants.

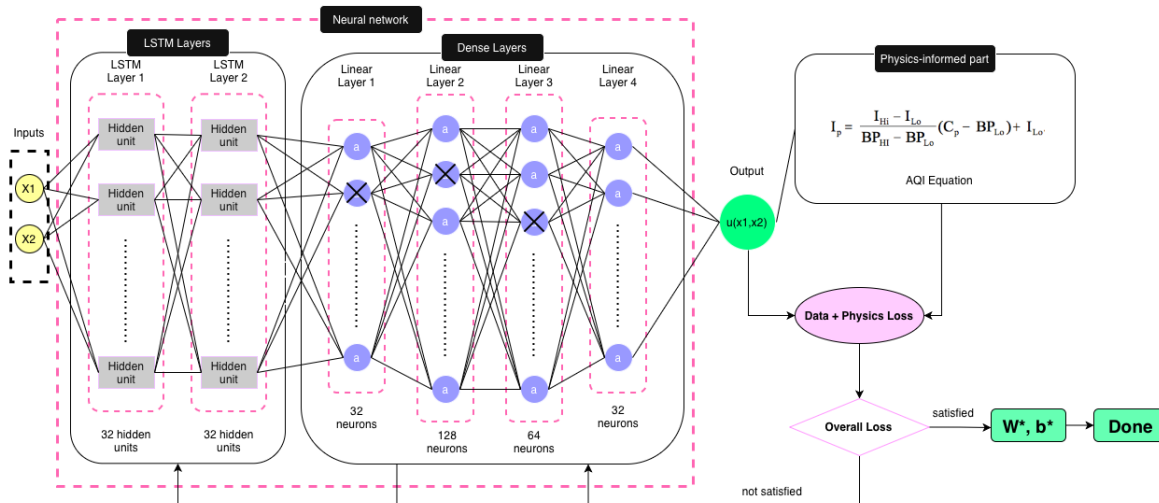


Figure 3: Architecture of the LSTM+Physics Model.

5 Experimental Setup and Evaluation Metrics

A unified experimental protocol was adopted to ensure fair and reproducible comparison across classical, machine learning, deep learning, and physics-guided models for multi-horizon AQI forecasting.

5.1 Hardware and Software Specifications

A personal CPU-based computing system with an Intel Core i5 processor and 8 GB of RAM is used for the experiment of this research study and all the models were implemented in PyTorch. The software environment was based on Python, with data preprocessing and classical models implemented using NumPy, Pandas, scikit-learn, and statsmodels. Neural network-based and physics-guided models were implemented using PyTorch. To ensure reproducibility, fixed random seeds were applied across all experiments, and all datasets were split chronologically to avoid temporal data leakage.

5.2 Model Hyperparameter Configuration

A concise summary of the hyperparameter settings is shown in the Table 4 which is used in the evaluated models. It represents the common architectural and optimization parameters that are used in the experiments. Classical models, including Linear Regression and SARIMAX, rely on fixed analytical formulations and therefore do not require iterative optimization or feature scaling.

5.3 Evaluation Metrics

To evaluate the forecasting performance of the proposed models, standard regression-based error metrics are used. These metrics quantify the difference between the predicted AQI values and the observed (true) AQI values on the test dataset. All evaluation metrics are computed in real AQI units to ensure clear interpretation and practical relevance.

Table 4: Generalized hyperparameter settings for all evaluated models

Hyperparameter	LR	SARIMAX	MLP	MLP+Physics	LSTM	LSTM+Physics
Architecture / Order	OLS	(1,1,1)×(1,0,1,7)	64-32	64-32	LSTM(32,32)+MLP	LSTM(32,32)+MLP
Activation	-	-	ReLU	ReLU	ReLU	ReLU
Optimizer	-	-	AdamW	Adam	Adam	Adam
Learning rate	-	-	0.001	0.001	0.001	0.001
Batch size	-	-	Full	Full	32	32
Scaling method	None	None	StandardScaler	StandardScaler	MinMaxScaler [-1, 1]	MinMaxScaler [-1, 1]

5.3.1 Mean Absolute Error (MAE)

Mean Absolute Error (MAE) measures the average magnitude of the prediction errors without considering their direction. It indicates how far, on average, the predicted AQI values deviate from the observed values and is less sensitive to large outliers.

$$\text{MAE} = \frac{1}{N} \sum_{i=1}^N |y_i - \hat{y}_i| \quad (9)$$

5.3.2 Mean Squared Error (MSE)

Mean Squared Error (MSE) computes the average of the squared differences between the predicted and observed AQI values. By squaring the errors, MSE penalizes larger prediction errors more heavily, making it useful for assessing model stability and robustness.

$$\text{MSE} = \frac{1}{N} \sum_{i=1}^N (y_i - \hat{y}_i)^2 \quad (10)$$

5.3.3 Normalized Mean Squared Error (NMSE)

Normalized Mean Squared Error (NMSE) is used to evaluate the prediction error relative to the variability of the observed AQI values. By normalizing the MSE with respect to the variance of the ground-truth data, NMSE allows fair comparison across different pollutants and forecasting horizons. Lower NMSE values indicate better predictive performance, while values close to or greater than 1 suggest poor model accuracy relative to the data variance.

$$\text{NMSE} = \frac{\frac{1}{N} \sum_{i=1}^N (y_i - \hat{y}_i)^2}{\frac{1}{N} \sum_{i=1}^N (y_i - \bar{y})^2} \quad (11)$$

Here, y_i denotes the observed AQI value, \hat{y}_i is the predicted AQI value, \bar{y} represents the mean of the observed AQI values, and N is the total number of samples.

6 Results & Comparative Analysis

This section presents the empirical performance of all of the forecasting models for two pollutants ($\text{PM}_{2.5}$ and O_3) and four forecasting horizons ($LAG \in \{1, 7, 14, 30\}$ days). We analyze, first of all, the behavior of the multi-horizon AQI targets to understand the changing difficulty in forecasting based on the time gap. Next, we are comparing baseline statistical and deep learning models (LR, SARIMAX, MLP, and LSTM). Finally, we test physics-guided variants (MLP+Physics and LSTM+Physics) and discuss the effect of the EPA breakpoint-based AQI constraint on the predictive accuracy and stability of the model for each pollutant and horizon.

6.1 Descriptive Analysis of Multi-Horizon AQI Targets

Figure 4 shows the relation between the present AQI at time t and the future goals at $t + 1$, $t + 7$, $t + 14$, and $t + 30$ in the case of $\text{PM}_{2.5}$ (top row) and O_3 (bottom row). With $LAG = 1$, the goals are still rather near to the current AQI. This indicates that there is a whole lot of short-term persistence and the forecast is pretty stable. As the AQI forecasting

horizons become closer to $LAG = 7, 14,$ and $30,$ the future AQI becomes less dependent on the present and more variable, which indicates that it is less dependent on time. As this disparity gets larger with respect to time, that is why prediction errors tend to go up.

For the case of $PM_{2.5},$ the AQI targets have much smoother and more gradual temporal changes. $PM_{2.5}$ shows rather stable features in all horizons, so it is more predictable as compared to $O_3.$ However, relatively along with it, O_3 have considerably higher daily swings, especially over longer time horizons, which implies O_3 AQI forecasting is less stable and tougher over longer time periods. Overall, the figure highlights the use of more expressive forms of learning (MLP/LSTM), the guidance of domains (physics constraints) to improve resilience, and the use of multi-horizon forecasting models.

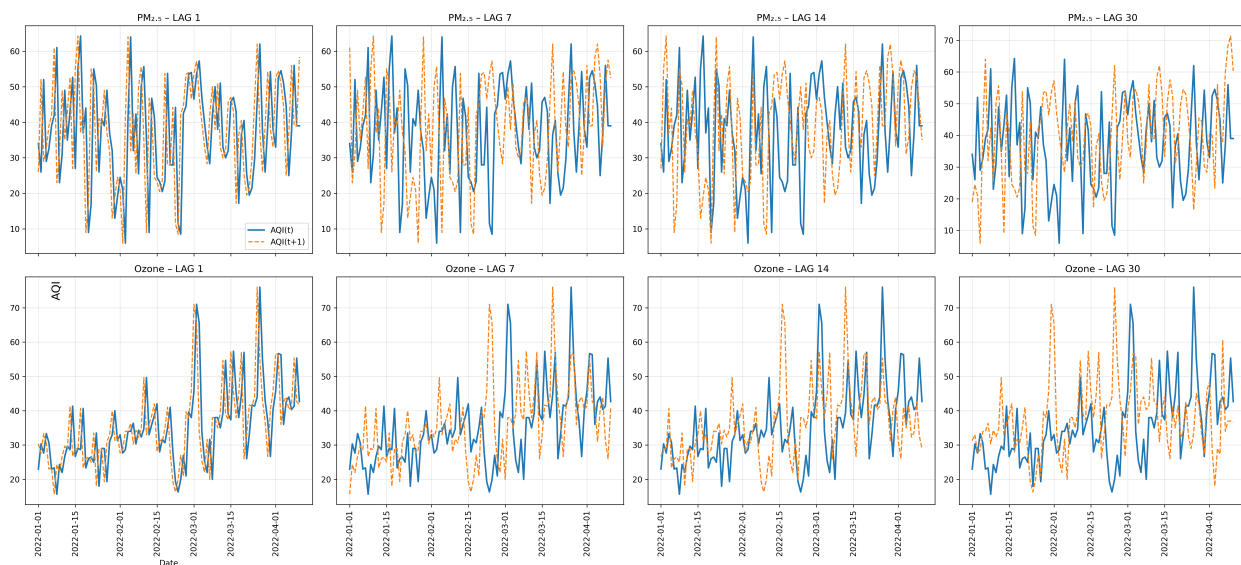


Figure 4: Multi-horizon AQI target visualization for $PM_{2.5}$ (top row) and O_3 (bottom row). Each subplot compares the current-day AQI (t) with future AQI values at 1, 7, 14, and 30-day LAG's prediction.

6.2 Baseline Model Performance Across Lag-Wise Data

We benchmark four baseline models such as linear regression (LR), SARIMAX, multilayer perceptron (MLP), and long short-term memory (LSTM) based on a lag-wise dataset of $PM_{2.5}$ and $O_3.$ For each pollutant and horizon, we provide the distribution of MAE, RMSE, and NMSE on the held-out chronological test set. These baseline results provide a point of reference for before this physics guidance is introduced.

6.2.1 $PM_{2.5}$ Baseline Results

Table 5 is a generalized benchmark of all the baseline performance on $PM_{2.5}.$ We found that the MLP and LSTM models provide lower error outcomes than the simple baselines if $LAG = 1,$ which suggests that nonlinear models are more useful to capture the pollutant AQI relationships. As when we increased the horizon to ($LAG = 7, 14,$ and $30),$ all models showed more or less efficiency, reflecting the increased uncertainty of longer-term forecasts. Among the baselines, LSTM is quite stable across horizons, which seems to indicate that sequence-based modeling performs better in generalization as the prediction gap becomes larger.

6.2.2 O_3 Baseline Results

Results for O_3 at the baseline appear in Table 6. Similar to $PM_{2.5},$ the smallest errors appear at $LAG = 1$ and the prediction errors grow as the horizons grow larger. MLP and LSTM roughly give better accuracy than simpler baselines, in line with their capacity to learn nonlinear patterns. Compared with $PM_{2.5},$ O_3 has more variation (Figure 4) and less performance in long horizons correspondingly. Overall, these results indicate that O_3 is more difficult to accurately predict for relatively long periods.

Table 5: Baseline performance of LR, SARIMAX, MLP, and LSTM models for PM_{2.5} AQI forecasting across all lag-wise datasets.

Model	LAG 1			LAG 7			LAG 14			LAG 30		
	MAE	RMSE	NMSE	MAE	RMSE	NMSE	MAE	RMSE	NMSE	MAE	RMSE	NMSE
LR	8.2803	10.7370	0.6646	10.2012	13.1408	0.9986	10.1016	12.6088	0.9894	10.2011	12.7831	1
SARIMAX	9.8861	12.9285	0.8967	31.7073	33.8115	0.9994	48.4128	50.1106	1	12.4783	15.2045	0.9999
MLP	8.2149	10.6535	0.6583	10.2289	13.1867	1.0305	10.0839	12.6538	1.0185	10.2548	12.8299	1.0464
LSTM	8.1761	10.6289	0.6552	10.0669	12.9638	0.9960	9.9955	12.5401	1.0003	9.9895	12.5433	1.0002

Table 6: Baseline performance of LR, SARIMAX, MLP, and LSTM models for O₃ AQI forecasting across all lag-wise datasets.

Model	LAG 1			LAG 7			LAG 14			LAG 30		
	MAE	RMSE	NMSE									
LR	12.8202	20.2004	0.6357	17.1723	25.9813	1	16.1777	24.0898	0.8936	17.7215	25.5043	0.9892
SARIMAX	15.5971	22.6346	0.8065	16.997	25.4225	0.9910	17.8621	25.4614	1	29.7733	33.3162	1
MLP	12.8785	20.2860	0.6451	17.4830	26.4023	1.0877	16.0078	23.8830	0.8860	17.4687	25.2393	0.9768
LSTM	12.7642	19.4974	0.5959	16.7570	25.2099	0.9917	16.3613	23.9691	0.8924	17.7549	25.3641	0.9865

6.3 Proposed Physics-Guided Model Performance Across Lag-Wise Data

The proposed physics-guided models (MLP+Physics and LSTM+Physics) are evaluated, which use the EPA breakpoint-based AQI mapping as a consistency constraint during the training. The goal would be to help increase predictive stability and allow for the physical meaning of pollutant-AQI relationships. We compare the results of physics-guided with the corresponding baseline models using MAE, RMSE, and NMSE for all horizons.

6.3.1 MLP+Physics Results

Multiple results from MLP+Physics obtained using different settings of loss weights ($\lambda_{\text{data}}, \lambda_{\text{phys}}$) are shown in frequencies in Table 7 and Table 8. For PM_{2.5} (Table 7) physics guidance is suggested to achieve small but consistent improvement over the baseline MLP for the majority of the horizons, with mainly significant improvement observed for the short horizon ($LAG = 1$). In addition, the use of balanced weighting (e.g., $\lambda_{\text{data}} = 0.5, \lambda_{\text{phys}} = 0.5$) may improve the performance at medium horizons; this would suggest that moderate guidance from physics may aid generalization in situations where the forecast gap becomes greater.

Table 7: Physics-guided MLP performance for PM_{2.5} across forecasting horizons with different λ_{data} and λ_{phys} settings.

Model	λ_{data}	λ_{phys}	LAG 1			LAG 7			LAG 14			LAG 30		
			MAE	RMSE	NMSE	MAE	RMSE	NMSE	MAE	RMSE	NMSE	MAE	RMSE	NMSE
MLP+Physics	0.0	1.0	8.1695	10.6349	0.6560	10.1783	13.1374	1.0228	10.0925	12.6804	1.0228	10.2176	12.7926	1.0404
MLP+Physics	0.3	0.7	8.1826	10.6395	0.6565	10.1934	13.1508	1.0249	10.1092	12.6937	1.0249	10.2260	12.8006	1.0417
MLP+Physics	0.5	0.5	8.1918	10.6430	0.6570	10.2015	13.1591	1.0262	10.0649	12.6396	1.0162	10.2332	12.8081	1.0429
MLP+Physics	0.7	0.3	8.2017	10.6477	0.6576	10.2152	13.1725	1.0283	10.0713	12.6445	1.0170	10.2399	12.8143	1.0439
MLP	1.0	0.0	8.2149	10.6535	0.6583	10.2289	13.1867	1.0305	10.0839	12.6538	1.0185	10.2548	12.8299	1.0464

For O₃ (Table 8) improvements are not as great and in some cases are comparable to the baseline MLP. This suggests that the breakpoint-based constraint may be less directly beneficial for O₃ for daily aggregated observations of observations where the variability of AQI is more significant. Figure 5 gives qualitative comparisons of the predicted and the true AQI on the test subset for both pollutants and shows that physics guidance can lead to more stable and less unrealistic fluctuations of the short-term forecasting behavior.

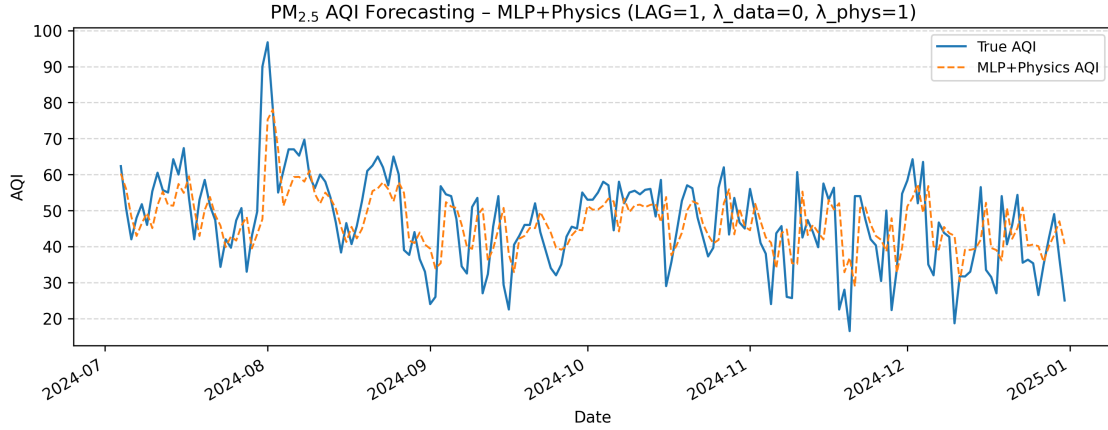
6.3.2 LSTM+Physics Results

Tables 9 and 10 show the performance of the LSTM+Physics model across all forecasting horizons and loss-weight configurations for PM_{2.5} and O₃, respectively.

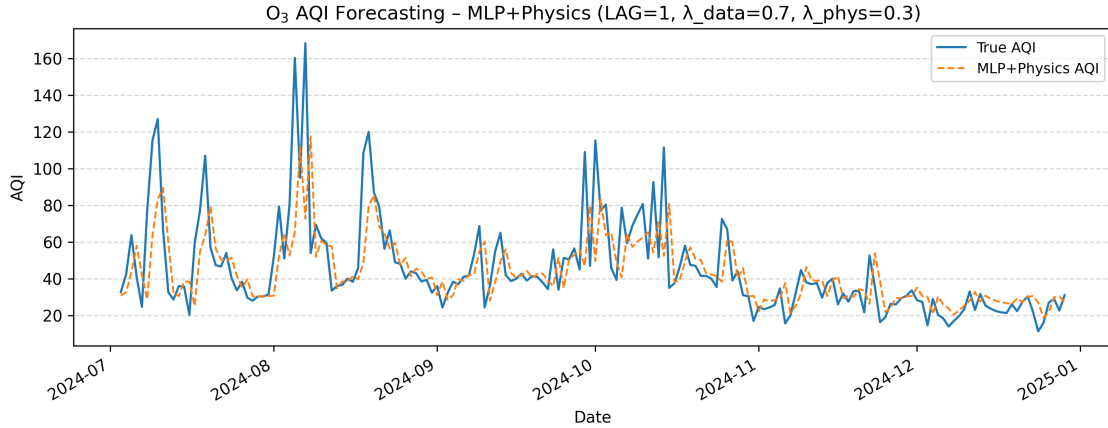
PM_{2.5} (Table 9), the proposed LSTM+Physics model realizes a good and more stable performance for all over AQI forecasting horizons. The trade-off between data loss and physics loss changes slightly depending on the forecasting

Table 8: Physics-guided MLP performance for O_3 across forecasting horizons with different λ_{data} and λ_{phys} settings.

Model	λ_{data}	λ_{phys}	LAG 1			LAG 7			LAG 14			LAG 30		
			MAE	RMSE	NMSE									
MLP+Physics	0.0	1.0	12.9227	20.2878	0.6452	17.5359	26.4362	1.0905	16.0406	23.8743	0.8853	17.5058	25.2256	0.9757
MLP+Physics	0.3	0.7	12.9086	20.2862	0.6451	17.5197	26.4273	1.0898	16.0338	23.8792	0.8857	17.4972	25.2312	0.9762
MLP+Physics	0.5	0.5	12.9000	20.2855	0.6451	17.5082	26.4238	1.0895	16.0278	23.8808	0.8858	17.4954	25.2322	0.9763
MLP+Physics	0.7	0.3	12.8913	20.2854	0.6451	17.4972	26.4139	1.0887	16.0212	23.8823	0.8859	17.4841	25.2338	0.9764
MLP	1.0	0.0	12.8785	20.2860	0.6451	17.4830	26.4023	1.0877	16.0078	23.8830	0.8860	17.4687	25.2393	0.9768



(a) $PM_{2.5}$ AQI forecasting using MLP+Physics on the test subset.



(b) O_3 AQI forecasting using MLP+Physics on the test subset.

Figure 5: Time-series comparison of true and predicted AQI values on the test set using the physics-guided MLP model for (a) $PM_{2.5}$ and (b) O_3 . The plots show the last portion of the test period to highlight short-term forecasting behavior.

horizon, though the differences, overall, between different weight settings are small. Such a result suggests that the LSTM sequence is more perfect and related to capturing most of the temporal dynamics, while the physics-based constraint mainly contributes to improving physical properties and changing the stabilization for predictions rather than drastically reducing error values. This behavior is supported graphically by Figure 6(a), where it can be seen that the predicted AQI closely follows the observed $PM_{2.5}$ AQI’s definite trajectory in the test subset.

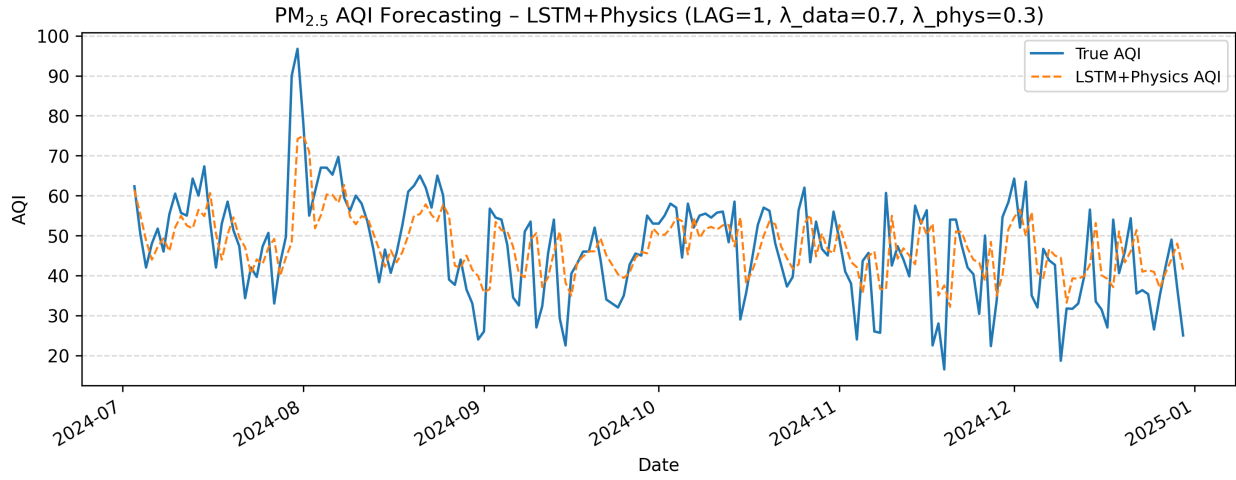
For O_3 (Table 10) the baseline LSTM is very competitive and generally the number of errors being fewer when the physics guidance was added is not evident for all horizons. Nevertheless, physics-informed training still has an important role to play by enforcing physically meaningful pollutant-AQI relations. As shown in Figure 6(b), the LSTM+Physics model captures the observed trends of the O_3 AQI trend well over time and does not show unrealistic fluctuations, which suggests the improved temporal stability of the model even with a lack of quantitative improvements.

Table 9: Physics-guided LSTM performance for PM_{2.5} across forecasting horizons with different λ_{data} and λ_{phys} settings.

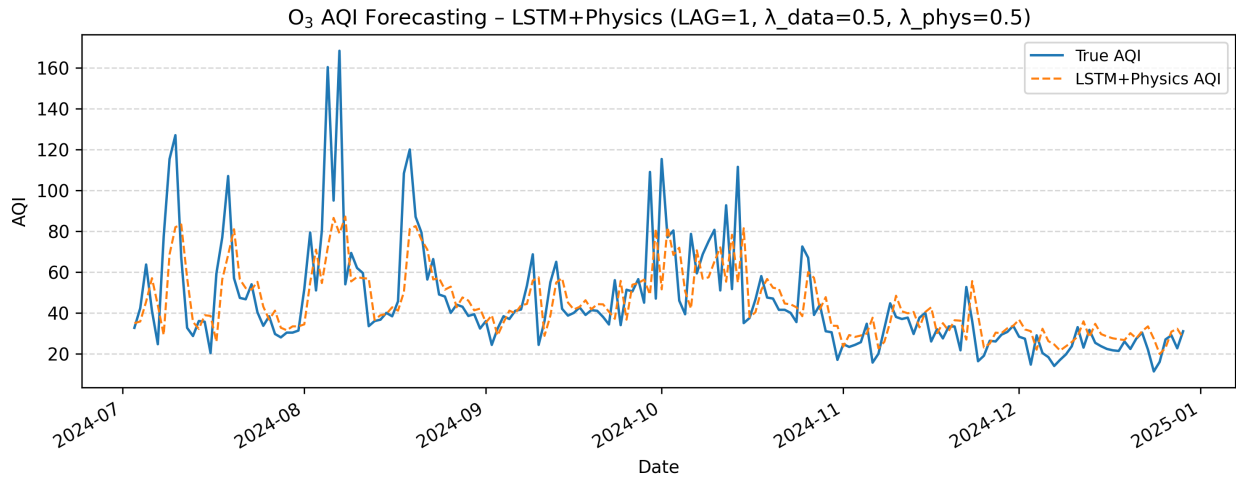
Model	λ_{data}	λ_{phys}	LAG 1			LAG 7			LAG 14			LAG 30		
			MAE	RMSE	NMSE	MAE	RMSE	NMSE	MAE	RMSE	NMSE	MAE	RMSE	NMSE
LSTM+Physics	0.0	1.0	8.1558	10.6348	0.6560	10.0467	12.9498	0.9938	9.9795	12.5423	1.0006	9.9896	12.5433	1.0002
LSTM+Physics	0.3	0.7	8.1943	10.6364	0.6562	10.0305	12.9414	0.9925	9.9807	12.5406	1.0004	9.9894	12.5433	1.0002
LSTM+Physics	0.5	0.5	8.1704	10.6322	0.6556	10.0403	12.9432	0.9928	9.9815	12.5398	1.0002	9.9902	12.5435	1.0002
LSTM+Physics	0.7	0.3	8.1639	10.6237	0.6546	10.0622	12.9576	0.9950	10.0042	12.5447	1.0010	9.9909	12.5438	1.0003
LSTM	1.0	0.0	8.1761	10.6289	0.6552	10.0669	12.9638	0.9960	9.9955	12.5401	1.0003	9.9895	12.5433	1.0002

Table 10: Physics-guided LSTM performance for O₃ across forecasting horizons with different λ_{data} and λ_{phys} settings.

Model	λ_{data}	λ_{phys}	LAG 1			LAG 7			LAG 14			LAG 30		
			MAE	RMSE	NMSE									
LSTM+Physics	0.0	1.0	12.7986	19.4895	0.5954	16.6970	25.2380	0.9939	16.4360	23.9733	0.8927	17.7256	25.3531	0.9856
LSTM+Physics	0.3	0.7	12.7856	19.5148	0.5970	16.6655	25.2851	0.9976	16.4991	23.9886	0.8938	17.8042	25.3755	0.9874
LSTM+Physics	0.5	0.5	12.8550	19.4646	0.5939	16.6616	25.2858	0.9977	16.4206	23.9859	0.8936	17.7970	25.3737	0.9872
LSTM+Physics	0.7	0.3	12.8602	19.4922	0.5956	16.6410	25.3056	0.9992	16.4376	23.9728	0.8926	17.7830	25.3708	0.9870
LSTM	1.0	0.0	12.7642	19.4974	0.5959	16.7570	25.2099	0.9917	16.3613	23.9691	0.8924	17.7549	25.3641	0.9865



(a) PM_{2.5} AQI forecasting using LSTM+Physics on the test subset.



(b) O₃ AQI forecasting using LSTM+Physics on the test subset.

Figure 6: Time-series comparison of true and predicted AQI values on the test set using the physics-guided LSTM model for (a) PM_{2.5} and (b) O₃.

6.4 Summary of Key Findings

For $PM_{2.5}$ at lag = 1, the LSTM+Physics (0.7, 0.3) achieves the best performance, at lag = 7, the LSTM+Physics (0.3, 0.7) achieves the lowest RMSE (12.9414) and NMSE (0.9925), and at lag = 14, the LSTM+Physics (0.5, 0.5) outperforms the rest. For lag = 30, the LSTM+Physics (0.3, 0.7) has the best overall performance. For the another pollutant O_3 at lag = 1, the LSTM+Physics (0.5, 0.5) achieves the best overall performance; at lag = 7, the baseline LSTM (1, 0) provides the lowest RMSE (25.2099) with competitive NMSE (0.9917); at lag = 14, the MLP+Physics (0, 1) yields the best performance and lag = 30, the MLP+Physics (0, 1) achieves the best overall results. From the observed results it could be stated that physics-guided deep-learning models improve the AQI forecasting accuracy. The LSTM+Physics model consistently performs best for $PM_{2.5}$ across all lags and also for short-term O_3 AQI prediction, while the MLP+Physics model generalizes better for long-term O_3 AQI forecasting.

For the set of both pollutants and all horizons, there are four conclusions that can be drawn. First, the difficulty of the forecast rises with the horizon, and in general, the performance decreases from $LAG = 1$ to $LAG = 30$, which is exactly what we want to see in the target behavior in Figure 4. Second, deep learning models (MLP and especially LSTM) generally are better than simple baselines. Third, physics guidance is the most unambiguous in terms of $PM_{2.5}$ particularly at short horizons, by making the stability of $PM_{2.5}$ more robust and enforcing physically meaningful pollutant-AQI consistency. Finally, LSTM-based models indicate the strongest performance over horizons, whereas the physical constraints can potentially allow further improvements in stability and interpretability based on the pollutant and horizon.

7 Discussion

This research study is an attempt to set an overall comprehensive benchmark of the classical, machine learning, deep learning, and knowledge-guided physics models for AQI multi-horizon forecasting in North Texas's Dallas County. Overall the experimental results point out a few significant pieces of information about the behavior of the experimented model, pollutant characteristics, and the role of knowledge guidance of physics.

First of all, the observed degradation in the overall performance for the AQI forecasting horizons with different lag increases is expected and in line with atmospheric dynamics. Short horizon AQI predictions have excellent temporal persistence, whereas longer time horizons have accumulated uncertainties due to meteorological variability and emission changes as well as nonlinear chemical interactions. This effect can be seen especially well in O_3 , which has more day-to-day volatility than $PM_{2.5}$. Secondly, deep learning models perform invariably better than the classical model used to baseline for pollutants and AQI forecast horizons. It is worth mentioning that the MLP captures the nonlinear relationship between pollutant concentration and the AQI, and the LSTM captures nonlinear relationships further and models the temporal dependencies. The higher stability with longer horizons of LSTM models shows that sequence-based learning is particularly effective when it comes to AQI forecasting tasks. Third, an EPA breakpoint-based AQI physics model incorporates the learning process, enhancing the model's behavior beyond just pure accuracy metrics. For $PM_{2.5}$, physics guidance offered greatly reduced errors and more stable predictions, especially for short-time forecasts. The data indicates that $PM_{2.5}$ is related to AQI in a much more direct and stable manner, which could be well reinforced using physics-based constraints. On the other hand, straight AQI physics limitations are less useful for O_3 forecasting. A simple breakpoint-based AQI calculation is not enough to consider the complicated photochemical reactions, weather, and precursor emissions required for ozone production. However, through not relying on irrational forecasts and maintaining physically consistent AQI trajectories with time, physics-guided models still hold qualitative advantages.

Overall, it can be seen that if there is a strong and clear physical relationship between inputs and targets such as in the case of $PM_{2.5}$, physics-guided learning works best. Physics guiding plays less of a direct and improving accuracy role and more of a stabilizing and regularizing mechanism when the background process is more complicated, like it is in the case of O_3 .

8 Conclusion

To improve accuracy and provide the standard for multi-horizon AQI forecasting in North Texas, Dallas County is represented in this research study by the use of EPA $PM_{2.5}$ and O_3 data. Classical statistical models, deep learning variants, and physics-guided variants were systematically tested on standardized lag-wise datasets to check their predictive accuracies, stability, and physical consistency.

The experimental results proved that deep learning models, especially LSTM, could successfully outperform the simpler baselines for all aspects of forecasting results with different forecasting horizons. Moreover, incorporating

EPA breakpoint-based AQI physics also ensured the results were more stable and physically plausible, and the most obvious improvement was seen in the results of $PM_{2.5}$ and short-term forecasts. For O_3 , physics guidance is more of a contribution to the stabilization of predictions than to a large reduction in the numerical error.

Overall, the results show that lightweight guides from physics can improve the deep learning-based AQI forecasting without introducing excessive complexity, and the effectiveness is related to pollutant characteristics and forecast time. This benchmark offers practical information for the selection and deployment of AQI forecasting models for urban applications of air quality.

Acknowledgments

This research has been conducted in the Data Driven Decisions (D3) Lab in the Anuradha and Vikas Sinha Department of Data Science at the University of North Texas.

References

- [1] Ankita Mishra and Yogesh Gupta. Comparative analysis of air quality index prediction using deep learning algorithms. *Spatial Information Research*, 32(1):63–72, 2024.
- [2] Sai Varun Chandrashekar, Firoz Khan, Sunaina Sridhar, Rajesh Kumar Dhanaraj, Balamurugan Balusamy, Dragan Pamucar, and Malathy Sathyamoorthy. A hybrid physics-informed neural and explainable ai approach for scalable and interpretable aqi predictions. *MethodsX*, page 103597, 2025.
- [3] Ramadoss Janarthanan, Pachaivannan Partheeban, K Somasundaram, and P Navin Elamparathi. A deep learning approach for prediction of air quality index in a metropolitan city. *Sustainable Cities and Society*, 67:102720, 2021.
- [4] Suresh Kumar Natarajan, Prakash Shanmurthy, Daniel Arockiam, Balamurugan Balusamy, and Shitharth Selvarajan. Optimized machine learning model for air quality index prediction in major cities in india. *Scientific reports*, 14(1):6795, 2024.
- [5] Anuradha Yenikar, Ved Prakash Mishra, Manish Bali, and Tabassum Ara. Explainable forecasting of air quality index using a hybrid random forest and arima model. *MethodsX*, page 103517, 2025.
- [6] Maziar Raissi, Paris Perdikaris, and George E Karniadakis. Physics-informed neural networks: A deep learning framework for solving forward and inverse problems involving nonlinear partial differential equations. *Journal of Computational physics*, 378:686–707, 2019.
- [7] Salvatore Cuomo, Vincenzo Schiano Di Cola, Fabio Giampaolo, Gianluigi Rozza, Maziar Raissi, and Francesco Piccialli. Scientific machine learning through physics-informed neural networks: Where we are and what's next. *Journal of Scientific Computing*, 92(3):88, 2022.
- [8] Byeongseong Choi and Michelle A Hummel. Spatiotemporal air quality prediction using stochastic advection-diffusion model for multimodal data fusion. *Environmental Research Letters*, 20(1):014065, 2025.
- [9] Zenglei Zhang, Chunqi Wang, Chunying Lin, Yi Wu, Jing Wei, Jiapeng Lu, Bowang Chen, Chaoqun Wu, Xiaoyan Zhang, Yang Yang, et al. Association of long-term exposure to ozone with cardiovascular mortality and its metabolic mediators: evidence from a nationwide, population-based, prospective cohort study. *The Lancet Regional Health-Western Pacific*, 52, 2024.
- [10] Stacey E Alexeeff, Kamala Deosaransingh, Stephen Van Den Eeden, Joel Schwartz, Noelle S Liao, and Stephen Sidney. Association of long-term exposure to particulate air pollution with cardiovascular events in california. *JAMA Network Open*, 6(2):e230561–e230561, 2023.
- [11] Sarawut Sangkham, Worrador Phairuang, Samendra P Sherchan, Nattapon Pansakun, Narongsuk Munkong, Kritsada Sarndhong, Md Aminul Islam, and Pornpun Sakunkoo. An update on adverse health effects from exposure to pm2. 5. *Environmental Advances*, 18:100603, 2024.
- [12] P Goyal, Andy T Chan, and Neeru Jaiswal. Statistical models for the prediction of respirable suspended particulate matter in urban cities. *Atmospheric environment*, 40(11):2068–2077, 2006.
- [13] Hamid Taheri Shahraini and Sahar Sodoudi. Statistical modeling approaches for pm10 prediction in urban areas; a review of 21st-century studies. *Atmosphere*, 7(2):15, 2016.
- [14] Hong Zhang, Sheng Zhang, Ping Wang, Yuzhe Qin, and Huifeng Wang. Forecasting of particulate matter time series using wavelet analysis and wavelet-arma/arima model in taiyuan, china. *Journal of the Air & Waste Management Association*, 67(7):776–788, 2017.

- [15] Tong Liu, Alexis KH Lau, Kai Sandbrink, and Jimmy CH Fung. Time series forecasting of air quality based on regional numerical modeling in hong kong. *Journal of Geophysical Research: Atmospheres*, 123(8):4175–4196, 2018.
- [16] Shruti Dadhich, Vibhakar Pathak, Rohit Mittal, and Ruchi Doshi. Machine learning for weather forecasting. *Machine Learning for Sustainable Development*, 10:9783110702514–010, 2021.
- [17] Xingyu Li, Long Li, Longgao Chen, Ting Zhang, Jianying Xiao, and Longqian Chen. Random forest estimation and trend analysis of pm2. 5 concentration over the huaihai economic zone, china (2000–2020). *Sustainability*, 14(14):8520, 2022.
- [18] Gokulan Ravindiran, Gasim Hayder, Karthick Kanagarathinam, Avinash Alagumalai, and Christian Sonne. Air quality prediction by machine learning models: A predictive study on the indian coastal city of visakhapatnam. *Chemosphere*, 338:139518, 2023.
- [19] Nairita Sarkar, Rajan Gupta, Pankaj Kumar Keserwani, and Mahesh Chandra Govil. Air quality index prediction using an effective hybrid deep learning model. *Environmental Pollution*, 315:120404, 2022.
- [20] Khalid Elbaz, Wafaa Mohamed Shaban, Annan Zhou, and Shui-Long Shen. Real time image-based air quality forecasts using a 3d-cnn approach with an attention mechanism. *Chemosphere*, 333:138867, 2023.
- [21] Anh Tuan Nguyen, Duy Hoang Pham, Bee Lan Oo, Yonghan Ahn, and Benson TH Lim. Predicting air quality index using attention hybrid deep learning and quantum-inspired particle swarm optimization. *Journal of big data*, 11(1):71, 2024.
- [22] Yue Hu, Yitong Ding, and Wenjing Jiang. Geographically aware air quality prediction through cnn-lstm-kan hybrid modeling with climatic and topographic differentiation. *Atmosphere*, 16(5):513, 2025.
- [23] Anil Utku, Umit Can, Mustafa Alpsülün, Hasan Celal Balıkçı, Azadeh Amoozegar, Abdulmuttalip Pilatin, and Abdulkadir Barut. Advancing air quality monitoring: Deep learning-based cnn-rnn hybrid model for pm2. 5 forecasting. *Atmosphere*, 16(9):1003, 2025.
- [24] Rongye Shi, Ji Luo, Nan Zhou, Yuxuan Liu, Chaopeng Hong, Xiao-Ping Zhang, and Xinlei Chen. Phy-apmr: A physics-informed air pollution map reconstruction approach with mobile crowd-sensing for fine-grained measurement. *Building and Environment*, 272:112634, 2025.
- [25] Lianfa Li, Roxana Khalili, Frederick Lurmann, Nathan Pavlovic, Jun Wu, Yan Xu, Yisi Liu, Karl O’Sharkey, Beate Ritz, Luke Oman, et al. Knowledge-informed deep learning to mitigate bias in joint air pollutant prediction. *Environment International*, page 109915, 2025.
- [26] U.S. Environmental Protection Agency. AirData Download Daily Data — Outdoor Air Quality Data. <https://www.epa.gov/outdoor-air-quality-data/download-daily-data>, 2025. [Accessed: 2025-11-01].
- [27] Douglas C Montgomery, Elizabeth A Peck, and G Geoffrey Vining. *Introduction to linear regression analysis*. John Wiley & Sons, 2021.
- [28] Narges Roustaei. Application and interpretation of linear-regression analysis. *Medical Hypothesis, Discovery and Innovation in Ophthalmology*, 13(3):151, 2024.
- [29] George EP Box, Gwilym M Jenkins, Gregory C Reinsel, and Greta M Ljung. *Time series analysis: forecasting and control*. John Wiley & Sons, 2015.
- [30] Stylianos I Vagropoulos, GI Chouliaras, Evaggelos G Kardakos, Christos K Simoglou, and Anastasios G Bakirtzis. Comparison of sarimax, sarima, modified sarima and ann-based models for short-term pv generation forecasting. In *2016 IEEE international energy conference (ENERGYCON)*, pages 1–6. IEEE, 2016.
- [31] Fahad Radhi Alharbi and Denes Csala. A seasonal autoregressive integrated moving average with exogenous factors (sarimax) forecasting model-based time series approach. *Inventions*, 7(4):94, 2022.
- [32] Chae-Yeon Lee, Ju-Yong Lee, Seung-Hee Han, Jin-Goo Kang, Jeong-Beom Lee, and Dae-Ryun Choi. Performance evaluation of pm2. 5 forecasting using sarimax and lstm in the korean peninsula. *Atmosphere*, 16(5):524, 2025.
- [33] Marius-Constantin Popescu, Valentina E Balas, Liliana Perescu-Popescu, and Nikos Mastorakis. Multilayer perceptron and neural networks. *WSEAS Transactions on Circuits and Systems*, 8(7):579–588, 2009.
- [34] Kumar Abhishek, Maheshwari Prasad Singh, Saswata Ghosh, and Abhishek Anand. Weather forecasting model using artificial neural network. *Procedia Technology*, 4:311–318, 2012.
- [35] Hassan Al Sukhni, Fatma Sakr, Mutasem K Alsmadi, Magdy Abd-Elghany, Ibrahim A Gomaa, Shaimaa Abdallah, et al. Data-driven weather prediction: Integrating deep learning and ensemble models for robust weather forecasting. *Journal of Cybersecurity & Information Management*, 15(2), 2025.
- [36] Sepp Hochreiter and Jürgen Schmidhuber. Long short-term memory. *Neural computation*, 9(8):1735–1780, 1997.

- [37] Alex Graves. Long short-term memory. *Supervised sequence labelling with recurrent neural networks*, pages 37–45, 2012.
- [38] Rui Yan, Jiaqiang Liao, Jie Yang, Wei Sun, Mingyue Nong, and Feipeng Li. Multi-hour and multi-site air quality index forecasting in beijing using cnn, lstm, cnn-lstm, and spatiotemporal clustering. *Expert Systems with Applications*, 169:114513, 2021.
- [39] Huijun Zhang, Yaxin Liu, Chongyu Zhang, and Ningyun Li. Machine learning methods for weather forecasting: A survey. *Atmosphere*, 16(1):82, 2025.
- [40] U.S. Environmental Protection Agency. Technical assistance document for the reporting of daily air quality – the air quality index (aqi). Technical Report EPA-454/B-24-002, U.S. Environmental Protection Agency, Office of Air Quality Planning and Standards, Air Quality Assessment Division, Research Triangle Park, NC, 2024. Accessed: YYYY-MM-DD.